ELSEVIER

Journal of Electron Spectroscopy and Related Phenomena 106 (2000) 207–220

JOURNAL OF ELECTRON SPECTROSCOPY and Related Phenomena

www.elsevier.nl/locate/elspec

Dynamic localization of inner-shell excitations in free atomic and molecular clusters

A.A. Pavlychev[a,*], E. Rühl[b,**]

[a]*Institute of Physics, St. Petersburg State University, St. Petersburg 198904, Russian Federation*
[b]*Fachbereich Physik, Universität Osnabrück, Barbarastr. 7, D-49069 Osnabrück, Germany*

Abstract

Experimental and theoretical results on core-excited variable-size atomic and molecular clusters are reported. Rydberg excitations in rare gas clusters serve to study core–hole localization phenomena in weakly bound atomic systems. Specifically, 3s excited variable size argon clusters exhibit distinct shifts of the 3s→*n*p window resonances converging to the Ar 3s ionization threshold. These shifts are assigned on the basis of the quasiatomic approach, considering the influence of nearest neighbors as well as long range effects on the Ar 3s→*n*p Rydberg series. Experimental results on 1s-excited nitrogen- and carbon monoxide-clusters show almost identical spectra compared to the bare molecules and the solid. A significant blue-shift of the σ* shape-resonance relative to the isolated molecule is found in homogeneous nitrogen clusters and in the solid, whereas no shifts are observed in CO-clusters. These results are rationalized by using the quasiatomic approach in terms of differences in dynamic localization of core-excitations in the regime of σ* shape-resonances.

1. Introduction

Free clusters have received considerable attention recently since they are known to bridge the gap between the gas phase and condensed phase of matter [1,2]. The geometric and electronic structure of variable size clusters reflect size dependent properties of matter, which are suitably investigated by inner-shell excitation [3–5]. Increasing step by step the number of atoms N embodied in a cluster X_N leads finally to the transformation into the solid state (X_N, with $N=\infty$).

Several studies on rare gas clusters have been performed in the past using vacuum ultraviolet radiation [6–13] as well as soft and hard X-rays [3–5,14–20]. The main spectral changes that are observed as a function of cluster size are bracketed by the atoms on one hand and the condensed phase on the other hand. Condensed phase spectra are dominated by bulk excitations, whereas surface excitations occur preferentially in clusters because of their high and variable surface-to-bulk ratio. Several inner-valence and core excitation edges of free rare gas clusters have been investigated in the past, such as Ar 3s [6,7,12,13], Ar 2p [4,5,14], Ar 1s [3,16], Ne 1s [15], and Kr 3d [19,20]. These studies show the systematic conversion of atomic Rydberg states into the corresponding exciton states in the solid, where in free clusters often a mixture of surface and bulk resonances is observed. These are shifted in energy with respect to the corresponding atomic transitions, reflecting the influence of changes in polarization and screening effects in clusters. A clear correlation

*Corresponding author.
**Also corresponding author.

0368-2048/00/$ – see front matter
PII: S0368-2048(99)00078-X

between atomic one electron $n_0 l_0 \rightarrow nl$ transitions and the corresponding exciton states in the solid become evident with increasing cluster size, which is due to: (i) strong dynamic core–hole localization and (ii) strong energy separation of low lying atomic Rydberg transitions in the core-excitation regime. In contrast to the lowest Rydberg transitions, higher lying Rydberg states with larger radius and higher orbital momentum l show a different behavior since their dispersion is expected to be much more complicated as a result of the radial inhomogeneity and anisotropy of the cluster potential [21].

The core excitation regime of molecules is dominated by intense transitions into unoccupied valence orbitals, which are located either below or above the core ionization thresholds [22]. Shape resonances dominate the absorption cross sections in the core ionization continua [22,23]. These broad features are often treated as one-electron phenomena [24], since they are either associated with transitions from core levels to virtual molecular orbitals lying in core ionization continua [25] or with trapping of the ejected electron by the molecular cation potential [26]. Important properties of continuum resonances are related to core–hole localization and core–hole symmetry breaking: Recent studies on resonant inelastic X-ray scattering [27,28] and angular distributions of photoelectrons from N_2 and CO_2 [29,30] show evidence for different localization of the N and O 1s-shell excitations. It is found that the N $1s^{-1}$-states in nitrogen are delocalized, whereas the O $1s^{-1}$-states in carbon dioxide are localized. Such differences in localization are found to be associated with different relaxation behavior of core-excited molecular ions. Differently conditioned changes in atomic motion after core-excitation serve to investigate dynamic properties of shape resonances [30]. These are expected to play an important role in molecular clusters, especially since the equivalence of atomic sites in free molecules, such as in nitrogen, is disturbed by the low symmetry cluster potential.

Excitations in the solid state are usually described by delocalized Bloch functions, which can in turn be traced back into localized excitations in the atom. As a result, the localization and size dependence of excitations are closely related. Size dependent properties of core-excited states in variable size compounds consisting of equivalent or quasi-equivalent atomic sites give the perspective to understand in greater detail core hole localization and core–hole symmetry breaking phenomena in matter. The latter aspect has discussed recently in the context of resonant X-ray emission spectroscopy [31,32]. This is the motivation of the present work, where the localization of excitations in variable size rare gas clusters and molecular clusters is studied. We report both, experimental and theoretical results on size dependent properties of $3s^{-1}np$ excited in argon clusters Ar_N, 1s-excited nitrogen clusters $(N_2)_N$, as well as C 1s- and O 1s-excited carbon monoxide clusters $(CO)_N$. The results are also compared with properties of the isolated molecules and the condensed phase. Finally, the theoretical model, which is based on the quasi atomic (QA) approach [30,33,34] is applied in order to make predictions on size dependent changes in electronic and dynamic properties of C 1s- and O 1s-excited carbon dioxide clusters.

2. Experimental

The experimental setup consists of a molecular beam experiment which has been described earlier in detail [35]. It is mounted behind the exit slit of various soft X-ray monochromators. For the present study we used the following beam lines at the storage ring BESSY-I: TGM-7 (20–100 eV) [36] and HE-TGM-II (200–600 eV) [37]. The energy resolving power ($E/\Delta E$) of these beam lines is typically on the order of 300–500. It decreases with photon energy reaching $E/\Delta E \approx 200$ in the O 1s regime, since the 1000 l/mm-grating, that was used for the present work, is not optimized for high photon energies. Clusters are formed in the supersonic jet expansion using a nozzle diameter of 50 μm. Homogeneous clusters are obtained by expanding neat gases, whereas heterogeneous clusters are obtained from expansions of gas mixtures of defined mixing ratio. Variable size clusters are obtained by changing the expansion conditions of the jet. This is done most efficiently by changing the stagnation pressure p_0 and the stagnation temperature T_0. The average cluster size $\langle N \rangle$ is changed adjusting the stagnation temperature T_0 of the nozzle expansion,

while keeping the stagnation pressure constantly at typically 4–5 bar. However, this quantity is only accessible for atomic clusters, where $\langle N\rangle$ is obtained by calculating the reduced scaling parameter Γ^* [38], which is correlated with $\langle N\rangle$, according to earlier work [39,40]. As a result, argon clusters up to $\langle N\rangle = 750$ are obtained with the present setup [4]. However, this method does not work properly for molecular clusters, since cooling of the internal degrees of freedom of the molecular species cannot be controlled easily [41]. Therefore, we can only rely in the case of molecular clusters on maximum cluster sizes $N_{\max}$, which are obtained from time-of-flight mass spectra (cf. [17]). $N_{\max}$ is sensitive to the onset of cluster formation, but for inner-shell excitation this quantity is regarded as a lower limit of $\langle N\rangle$, since massive fragmentation leads to the formation of small fragment ions upon fission of the multiply charged clusters which are formed after core excitation. In the case of homogeneous molecular clusters we assume that $\langle N\rangle < 100$ for the conditions used in the present study, corresponding to $N_{\max} = 30$ at $T_0 =$ 170 K and $p_0 = 5$ bar [17].

The skimmed jet is crossed with the monochromatic soft X-ray beam in the ionization region of a time-of-flight mass spectrometer. Cations are formed upon photoionization, which are mass-selected in the time-of-flight mass spectrometer. Electrons are extracted into opposite direction into a total electron detector, consisting of a channeltron which is mounted in 1 cm distance from the ionization region.

Total electron yield spectra of solid samples are obtained by using a ultrahigh vacuum setup (base pressure: $5\cdot10^{-10}$ mbar), which is equipped with a cold head, which is kept at 25 K using a closed cycle helium refrigerator [20]. The gaseous samples are condensed on a sapphire platelet, which is equipped with two gold electrodes. Total electron yields are measured by using an additional electrode which is mounted in 1 cm distance from the condensed sample. The molecular films are slowly dosed on the platelet and are annealed by gentle heating before exposure to the X-ray beam.

The gaseous sample gases are of commercial quality (Linde, Germany). They are used for the present study without further purification (Ar, N_2, and CO: purity: >99.99%).

3. Theoretical

The QA approach [30,33,34] allows to describe spectral and angular dependences of inner-shell photoprocesses in terms of strongly localized atomic-like orbitals in free molecules [42,43]. It is assumed that the processes are initiated in one of the atomic sites that are located in the compound or cluster. The electron optical properties of the surroundings of the core-excited atom, such as reflectivity, transmission, refraction, and the photoelectron loss function, cause changes in the spectral and angular dependence of atomic photoprocesses. A pseudopotential concept is used in order to calculate the characteristic properties of the surroundings of the absorbing center [44]. The series of QA equations describing the amplitudes of electron waves which are reflected from the surroundings $B_{lml'm'}(E, b)$ or transmitted through the surroundings $T_{lml'm'}(E, R_{\mathrm{mol}})$ are obtained from an application of the variable phase approach [45,46], according to Refs. [33,34]:

$$B' = [\Phi^+ + B\Phi^-]W[\Phi^+ + \Phi^- B] \quad (1)$$

$$T' = -T\Phi^+ W[\Phi^+ + B\Phi^-], \quad (2)$$

where E is the kinetic energy of the photoelectron, l and l' are the photoelectron orbital momenta before and after the interaction with the surroundings potential, m and m′ are their projections, R_{mol} is the radius of the region inside which the reflected waves are formed, b is the radius of atomic core, $B = \{B_{lml'm'}(E, r)\}$, $T = \{T_{lml'm'}(E, r)\}$, $B' = \{\partial B_{lml'm'}/\partial r\}$, $T' = \{\partial T_{lml'm'}/\partial r\}$, and W is the interaction matrix. Its elements are $W_{lml'm'}(r) = \Sigma_\mu W_\mu(r)\int Y_{lm}(\Omega)Y_\mu(\Omega)Y_{l'm'}(\Omega)Y_{l'm'}(\Omega)\mathrm{d}\Omega$, where W_μ is the 2^μ-pole momentum of the surroundings potential, and $Y_{lm}(\Omega)$ is a spherical function centered at the excited atom. $\Omega^\pm$ are diagonal matrices, their non-zero elements are partial radial wave functions outgoing from and incoming into the excited atom, respectively. The border conditions $B(r > R_{\mathrm{mol}}) = 0$ (for Eq. (1)) and $T(r \approx b) = 1$ if $l = l_0 \pm 1$ and $T(r \approx b) = 0$, if $l \neq l_0 \pm 1$ (for Eq. (2)). Strong core–hole localization and core–hole symmetry breaking are postulated, if the time dependence of the core-excitations is neglected: The core-excited atom is regarded as a ‘point defect’ which is incorporated in a crystal

lattice or in a molecule. The QA model gives, therefore, a perspective to take core–hole delocalization into account by including the time evolution of strongly localized core-excitations, as will be shown in the following.

4. Results and discussion

4.1. Argon clusters

Fig. 1 shows a series of total electron yield spectra (TEY). The bottom spectrum represents the TEY of the atomic beam (Fig. 1(a)). The spectrum is dominated by a series of window resonances corresponding to Ar 3s→*n*p Rydberg transitions, which converge to the Ar 3s ionization energy at 29.240 eV [6,47]. The shape of the window resonances reflects the strong coupling of the Rydberg states with the underlying Ar 4p continuum. Fig. 1(b) corresponds to a TEY spectrum which is recorded at expansion conditions corresponding to $\langle N\rangle = 750$. It is similar in shape as the atomic TEY, but there occurs a broad feature at 27.6 eV. These relatively small size dependent changes are a result of the fact that the atomic window resonances have a considerably higher absorption cross section than the corresponding features in the solid [48]. Therefore, the TEY spectra of clusters indicate that a large fraction of the jet consists of clusters. The atomic contribution is subtracted from the raw TEY spectra in order to observe changes in the electronic structure as a function of the average cluster size $\langle N\rangle$. The resulting spectra are shown in Fig. 1(c)–(e). The energy positions of the dominant spectral features and spectral assignments are listed in Table 1. These indicate the occurrence of low lying broad features between 26.6 eV and 27.2 eV, as found in earlier work on mass-selected cluster cations (cf. [6,21]). These features are consequently assigned to surface excitations. A dominant window resonance is found between 27.8 eV (see Fig. 1(c)) and 27.6 eV (see Fig.

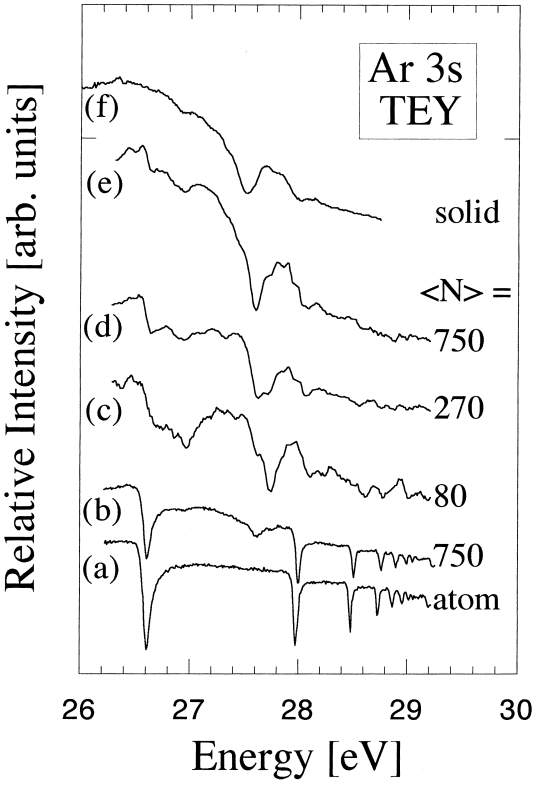

Fig. 1. Total electron yield spectra of (a) atomic argon, (b) $\langle N\rangle = 750$; (c)–(e) after subtraction of the atomic component at $\langle N\rangle = 80$, 270, and 750, respectively; (f) total electron yield spectrum of solid argon.

Table 1
Assignment of the low lying spectral features occurring in the Ar 3s excitation regime of atomic argon, variable size argon clusters of different average cluster size $\langle N\rangle$, and solid argon (cf. Fig. 1). Further details are given in the text

Absorbing species	Energy/eV	Assignment
Atom	26.61	$3s^{-1}4p$
	27.98	$3s^{-1}5p$
$\langle 80\rangle$	26.71	$3s^{-1}4p_{surf.\ (norm.)}$
	26.96	$3s^{-1}4p_{surf.\ (tang.)}$
	27.64	$3s^{-1}4p_{bulk}$
	27.75	$3s^{-1}5p_{surf.}$
	28.12	$3s^{-1}5p_{bulk}$
$\langle 270\rangle$	26.64	$3s^{-1}4p_{surf.\ (norm.)}$
	26.94	$3s^{-1}4p_{surf.\ (tang.)}$
	27.63	$3s^{-1}4p_{bulk}$
	27.72	$3s^{-1}5p_{surf.}$
	28.07	$3s^{-1}5p_{bulk}$
$\langle 750\rangle$	26.64	$3s^{-1}4p_{surf.\ (norm.)}$
	26.96	$3s^{-1}4p_{surf.\ (tang.)}$
	27.61	$3s^{-1}4p_{bulk}$
	28.05	$3s^{-1}5p_{bulk}$
Solid	27.51	$3s^{-1}4p_{bulk}$
	28.01	$3s^{-1}5p_{bulk}$

1(e)), a higher lying weak feature is observed between 28.12 eV (see Fig. 1(c)) and 28.05 eV (see Fig. 1(e)). This is similar to the TEY spectrum of the solid (Fig. 1(f)). However, the spectra displayed in Fig. 1(c)–(e) clearly indicate that they are not identical to that of the solid since all features that are assigned to bulk excitations in clusters occur at higher energy than in the solid. These have not quite the properties of the condensed phase, as will be shown below in combination with model calculations using the quasiatomic approach.

The behavior of the atomic $3s^{-1}np$ excitations ($n=4$, 5, 6) is computed as a function of the surroundings impact parameter λ [33,34] (see Fig. 2, dashed lines), which contains only short range effects. λ is in general a formal parameter, which can be interpreted as follows: $\lambda \sim \lambda_0^{-1}\Sigma_s\ (N_s\ c/R_s^2)\langle\rho_{nl}, s\rangle$, where N_S is the number of atoms in the s^{th} coordination shell of the cluster, R_s corresponds to its radius, c is the scattering length for the neighboring atom, $\langle\rho_{nl}, s\rangle$ is the electron density at the shell, and λ_0 is a normalization factor. λ is defined to be equal to zero for the isolated atom and equals to one for an atom that is located in the bulk. Its variations highlight how atomic excitations convert into excitons in the solid with increasing surroundings potential. The variation of λ is illustrated for Ar_{923}, which consists of seven shells in its perfect icosahedral geometry. The surface layer corresponds to $\lambda=0.4$, the next inner shells give the following increase in λ: 0.7, 0.9, and 0.98. The inner core of the cluster consists of three shells, with $\lambda=1$. Atoms inside the third coordination shell are consequently treated identically in order to consider long-range order effects. Additionally, an effective shielding of the Coulomb potential at the distance r is considered since the used pseudopotential of neighboring atoms is not able to account for dipole-induced interactions between rare-gas atoms in the clusters. This results in a constant potential outside the third coordination shell providing a decrease in Ar 3s-ionization potential at the transition from free atoms to solid argon. The energy dependencies for the $3s^{-1}4p$ and $3s^{-1}5p$ excitations on λ are computed with this potential that accounts for long range effects (cf. solid lines in Fig. 2). These indicate a more complex behavior than the short range effects. The common energy scale in Fig. 2 is referenced to the corresponding vacuum energy.

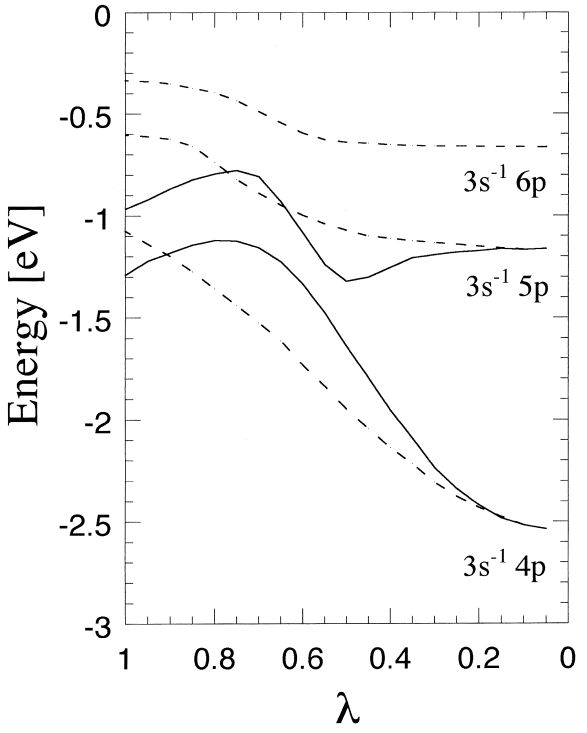

Fig. 2. The conversion of Rydberg Ar $3s^{-1}4p$ and $3s^{-1}5p$ excitations into the excitons of solid argon as a function on the surroundings parameter λ. The zero point of the common energy scale corresponds to the appropriate vacuum level. See text for further details.

The experimental results on free argon clusters indicate a complex evolution of the atomic $3s^{-1}np$-excitations as a function of the average cluster size $\langle N\rangle$. The calculated conversion (Fig. 2, dashed lines) of the $3s^{-1}np$ states as a function of the surroundings impact parameter λ with respect to the first coordination shell demonstrates that the $3s^{-1}np$ excitations evolve in terms of continuous blue-shifts as a function of the λ-parameter, i.e. cluster size. This is similar to earlier work of Wörmer et al., who used an exciton model that was related to fluorescence excitation experiments [12,13]. The present work shows that the shift in energy is largest for the lowest ($n=4$) excitation and drops quickly for higher principal quantum number n as the influence of nearest neighbors on Rydberg states with large radii decreases. Any reversal of this behavior is not found on the basis of short range effects. This implies within

the approximations that the excitations of higher Rydberg states in clusters can be assigned to transitions into antibonding cluster states. In addition, the calculations also indicate that there is a splitting δ of the surface resonances into a normal ($3s^{-1}np_{norm.}$) and tangential ($3s^{-1}np_{tang.}$) component. The $3s^{-1}np_{norm.}$ corresponds to the lowest energy component whereas the $3s^{-1}np_{tang.}$ represents the highest energy component, which is slightly dependent on the cluster size. δ equals 0.28 eV, 0.18 eV, and 0.06 eV for $n=4$, 5 and 6, respectively. A comparison with the experimental data (cf. Fig. 1 and Table 1) shows that such splitting is observed, corresponding to the lowest energy transitions in the 26.6–27.0 eV regime. However, we have to conclude that on this level of theory, the computed conversion of the atomic states into excitations of the bulk cannot explain reasonably the experimentally observed dependence of the $3s^{-1}np$ excitations as a function of $\langle N\rangle$. Evidently, long-range effects on the conversion of atomic Rydberg states into bulk excitations must be considered and demonstrate that the spectral changes are due to changes in λ. A non-monotonous behavior of the resonances energies results in relative red-shifts of both $3s^{-1}4p$ and $3s^{-1}5p$ resonances, especially in the regime of $\lambda>0.8$, i.e. in the bulk excitation regime. This is in agreement with the experimental results (cf. Fig. 1 and Table 1). For small values of λ the energy of the lowest excitation ($3s^{-1}4p$) increases while that of the $3s^{-1}5p$ decreases (cf. Fig. 2, solid lines). As a result, it is expected that both resonances approach each other as a function of $\langle N\rangle$. For larger λ the behavior of the $3s^{-1}5p$ resonance changes and a crossing of both levels does not appear. For values of λ that are close to 1 this separation is about 0.35 eV, which is in general agreement with the experimental results. This non-monotonous dependence is determined from the radial inhomogeneity of surroundings potential at large r. Finally, the conversion of the $3s^{-1}6p$ state cannot be examined separately with respect to higher-lying excitations and requires more detailed investigations.

In summary, the model calculations give detailed information on the evolution of resonant excitations in the Ar 3s regime as a function of cluster size, which agrees with the experimental findings: (i) The broad features at $\approx$26.6 eV and $\approx$26.9 eV are due to the $3s^{-1}4p$ surface excitation. The $3s^{-1}5p$ surface component is found at $\approx$27.75 eV. Both features lose intensity as $\langle N\rangle$ is increased. (ii) The bulk excitations are found at $\approx$27.6 eV ($3s^{-1}4p$) and $\approx$28.1 eV ($3s^{-1}5p$), respectively. Both features increase in intensity and approach the bulk limits with increasing $\langle N\rangle$. Table 1 contains a summary of the experimental results and assignments that are in agreement with the results based on the quasiatomic approach.

Often a clear correlation between an atomic $n_0l_0^{-1}nl$ excitation and an exciton in the solid becomes evident with increasing cluster size. Especially, the Ar $2p_{3/2}^{-1}$ 4s-excitation [4,5] gives a typical example for the conversion of spatially strongly localized excited states [33,34]. This excitation is built up from the superposition of surface and bulk resonances in clusters. Both features are blue-shifted with respect to the corresponding atomic transitions and show intensity ratios which linearly depend on the ratio of the number of atoms on the surface and in the bulk. The blue-shifts of both resonances relative to the corresponding atomic transition energies are rationalized by the increasing electron gas temperature at adiabatic stressing of the atomic volume at the transition from isolated atom to the bulk [33,34]. As a result, the profile of the Ar $2p_{3/2}^{-1}$ 4s-excitation provides a sensitive probe for the cluster shape, the density of structural defects, and mechanisms of condensation [5]. This clear picture is in contrast to the Ar 3s excitation, which is due to: (i) the strong spatial localization of the 2p–4s transition, where the nearest neighbors dominate the effect of the surroundings, (ii) the strong energy separation of this transition for atoms located on the surface and in the bulk of clusters, and (iii) the non-degenerate final 4s-state allows to neglect the anisotropy of the surroundings. Going to high-lying atomic excitations with larger radius and with higher orbital momentum l their conversion is expected to be much more complicated because the radial inhomogeneity and local anisotropy of the cluster potential. This allows an additional splitting into normal and tangential components and their hybridization with other l' atomic states. Such behavior is expected to modify the energy dependence of these high-lying states with cluster size, such as in the Ar 3s regime. The conversion of excitations as a func-

tion of cluster size in the inner-valence and core excitation regime are of particular interest since they serve to obtain additional information on the local electron-optical properties of matter.

4.2. Molecular clusters

4.2.1. Nitrogen clusters

Fig. 3 shows a comparison of spectra of gaseous, clustered, and solid nitrogen recorded in the N 1s excitation regime (390–440 eV). The spectra are similar to each other indicating that the electronic structure of the molecule is almost unchanged in the gas, clusters, and in the condensed phase, as can be expected for molecular Van der Waals systems. The spectra are dominated by an intense N $1s\rightarrow 2p\pi_g(\pi^*)$-resonance, which is located at 400.96 eV [49]. High resolution spectroscopy of gaseous and condensed nitrogen indicates that the N $1s\rightarrow 2p\pi_g(\pi^*)$-resonance consists of vibrational fine structure [50–52]. There is no shift in energy between the gas and the solid, rather than slight changes in vibrational fine structure [51–53]. However, the vibrational fine structure cannot be resolved with the present setup. Above this main feature there are Rydberg transitions converging to the N 1s ionization energy ($IE(N\ 1s)_{gas}=409.9$ eV [54] $IE(N\ 1s)_{solid}=408.85$ eV [53]; $IE(N\ 1s)_{cluster}=409.4$ eV [55]), which are also not resolved. Broad features in the N is continuum occur in the isolated molecule near 415 eV and 419 eV, respectively [50]. The general shape of the continuum features is similar in the gas, homogeneous and heterogeneous nitrogen clusters, and in condensed molecules (cf. insert of Fig. 3). However, small but characteristic differences are observed in this spectral regime. These are determined from photo-ion yields of mass-selected cations. This technique needs to be applied in order to suppress the detection of unclustered molecules, which dominate the composition of the jet. This is unlike the formation of atomic clusters, where a considerably larger fraction of the jet is condensed in clusters which have a different electronic structure than the isolated atom, allowing the application of total yield experiments (cf. Fig. 1). In the case of nitrogen and its clusters, properties of the isolated molecule are visualized by the N^+-yield (cf. Fig. 3 bottom spectrum). This cation is predominantly formed in the N 1s continuum by fission of the doubly charged molecule, yielding high N^+-intensity in the N is continuum. Fig. 3 also contains photo-ion yields of $N_2\cdot Ar^+$ and $(N_2)_2^+$. Both cation yields are measured under similar expansion conditions (cf. Fig. 3). The heterodimer $N_2\cdot Ar^+$ is evidently a fragment of larger heterogeneous clusters containing both components N_2 and Ar. Unfortunately, the composition of the neutral precursors cannot be obtained in a quantitative way. Additional experiments using different mixing ratios between both components indicate that the N 1s edge gets weak for

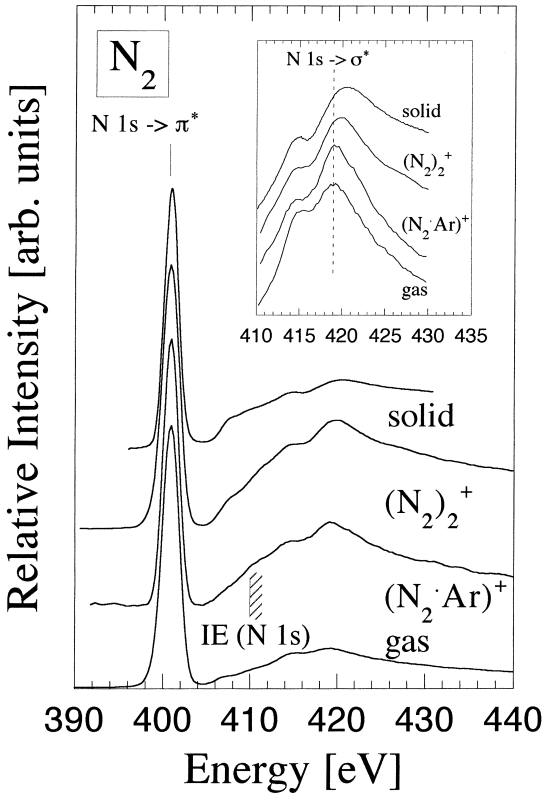

Fig. 3. The N 1s excitation regime of gaseous nitrogen (bottom, N^+-yield), nitrogen clusters (middle: heterogeneous nitrogen/argon clusters: $(N_2\cdot Ar)^+$-yield and homogeneous nitrogen clusters: $(N_2)_2^+$-yield), and solid nitrogen (top: total electron yield of multilayers). The insert shows the regime of the N $1s\rightarrow\sigma^*$ excitation. The vertical dashed line indicates the position of the N $1s\rightarrow\sigma^*$ shape-resonance in gaseous nitrogen. Experimental conditions of cluster formation: heterogeneous clusters: expansion of 9% Ar in N_2, $T_0=170$ K, $p_0=5$ bar; homogeneous clusters: expansion of neat N_2, $T_0=170$ K, $p_0=5$ bar.

mixtures containing less than 50% of N_2 [55]. This behavior may point to the fact that the molecular component is likely located in the bulk of the clusters. It is consistent with the finding that the Ar 2p regime of such mixtures is essentially similar in shape to homogeneous argon clusters [55]. The $(N_2)_2^+$-yield is obtained from expansions of neat nitrogen. It is also similar to the other yields shown in Fig. 3. Earlier work on homogeneous nitrogen clusters has shown that changes in the neutral cluster size distribution are reflected by an increase of the continuum features with growing neutral cluster size [17]. This behavior reflects changes in fragmentation mechanisms rather than changes in electronic structure. Intense core ionization continua in photo-ion yields reflect fission processes of primarily doubly charged clusters, which decay into singly charged small fragments. This effect is expected to become more prominent with increasing cluster size, if small fragment ions are selected for detection [17].

Small, but distinct differences in spectral shape are found in Fig. 3 (insert) in the regime of the N 1s→σ*-transition (419 eV in neat N_2). These changes are easily determined even with low spectral resolution. The results indicate that the N 1s→σ*-transition is narrower in the isolated molecule and in heterogeneous clusters ($N_2 \cdot Ar^+$) than in homogeneous clusters ($(N_2)_2^+$) and the condensed phase. In addition, there is also a characteristic blue-shift of ≈1 eV in homogeneous clusters that accompanies the broadening of this resonance. These results are also consistent with present (cf. Fig. 3) and earlier work on condensed nitrogen [56], where an even larger blue-shift of ≈1.5 eV is deduced. This result is interpreted from the experimental viewpoint that the N 1s→σ*-regime is sensitive to the local surroundings of the absorbing molecule in a cluster or in the condensed phase. The similarity of the molecular spectrum and the $N_2 \cdot Ar^+$-yield indicates that most likely isolated nitrogen molecules are contained in the heteroclusters, which are surrounded by argon. This explains also the finding that photo-ion yields of homogeneous clusters resemble the condensed phase spectra. However, a detailed understanding of the processes affecting the spectral shapes cannot be obtained on the basis of experimental results, as pointed out above for the Ar 3s regime. Therefore, a detailed analysis of the spectral shape in the regime of the N 1s→σ*-shape resonance is given below on the basis of the QA approach.

4.2.2. Carbon monoxide clusters

Fig. 4 shows the C 1s excitation regime of carbon monoxide (280–330 eV). Properties of the gaseous molecule are reflected by the total cation yield under conditions, where no clusters are present in the jet (bottom spectrum). C 1s excited carbon monoxide clusters are obtained by expanding the neat sample, yielding masses of cluster cations $(CO)_N^+$, reaching up to $N \approx 10$ (top spectrum in Fig. 4). The spectra are, as in the case of nitrogen, in general similar in shape. Minor differences are found in the C 1s continuum. There is a small, but visible shift of the feature near 293.3 eV, which is due to excitation of

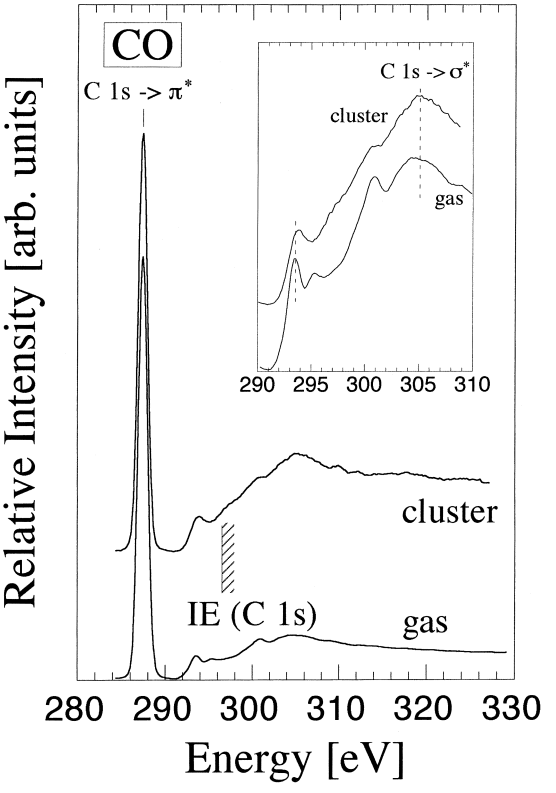

Fig. 4. The C 1s excitation regime of gaseous carbon monoxide (bottom, total cation yield, no clusters present in the beam: $T_0 = 300$ K, $p_0 = 4$ bar) and CO clusters (top: $(CO)_2^+$-yield: $T_0 = 170$ K, $p_0 = 4.3$ bar). The insert shows the regime of the C 1s→σ* excitation. The vertical dashed line near 305 eV indicates the position of the C 1s→σ*-resonance in gaseous CO.

the lowest p-Rydberg states in the molecule [57]. This feature is slightly blue-shifted and lower in intensity in the cluster cation yield. Similarly, the resonance which is observed in the molecular spectrum near 295 eV is not found in the cluster cation yield. These results are in line with earlier work on molecular clusters, where it is found that the intensity of Rydberg transitions is efficiently damped [58,59]. A blue-shift of these features is pointing to lower term values in clusters, especially since the core ionization energies are expected to be lowered in clusters compared to the gas phase molecules [55]. Another difference in shape between molecular and cluster properties is found near 300.7 eV, where a double excitation feature is found in earlier work [49]. This feature is expected to consist of multiple lines, which are related to the π*- and 5σ Rydberg-transitions of NO, similar to recent high resolution work on molecular nitrogen [50]. These features cannot be resolved, but decreased intensity in the cluster spectra indicates that this feature is likely to be related to double excitations involving Rydberg transitions. The C 1s→σ*-transition is located near 305 eV. Its shape is unchanged when comparing the gas phase spectrum with that of clusters. This is unlike the above mentioned results on nitrogen clusters. The O 1s excitation regime in molecular and clustered CO is shown in Fig. 5. Both spectra are almost identical in shape and there is no shift of the O 1s→σ* transition in clusters relative to the bare molecule. This is likely to some extent due to the poor spectral resolution in the O 1s regime (cf. Experimental Section). Therefore, subtle molecule-cluster shifts cannot be resolved with the present setup.

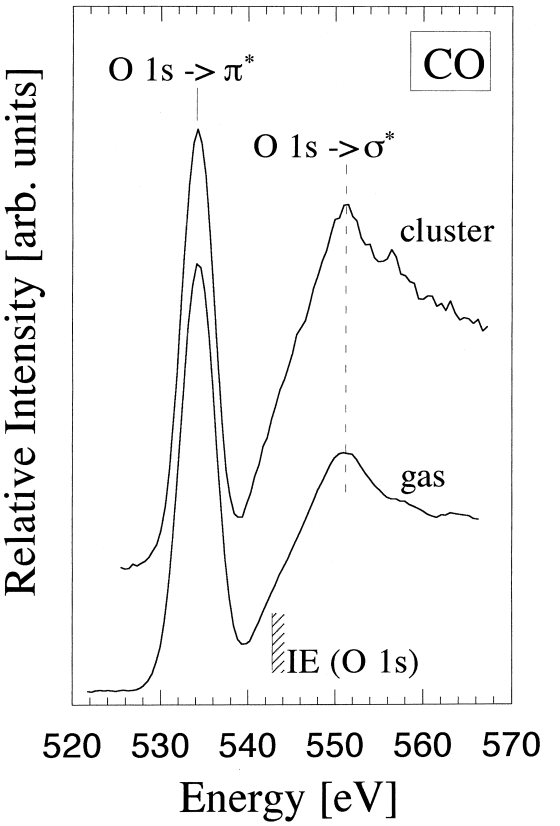

Fig. 5. The O 1s excitation regime of gaseous carbon monoxide (bottom, total cation yield, no clusters present in the beam: $T_0 = 190$ K, $p_0 = 1.5$ bar) and CO clusters (top: $(CO)_2^+$-$(CO)_{10}^+$-yield: $T_0 = 170$ K, $p_0 = 4.6$ bar). The vertical dashed line indicates the position of the O 1s→σ*-resonance in gaseous CO.

4.2.3. Dynamic properties of σ shape-resonances*

Excitations into unoccupied molecular orbitals, such as the N 1s→π*-transition and N 1s→σ* shape-resonance are tightly connected with the atomic N 1s→2p transition. Therefore both transitions are strongly spatially localized within the molecular system, which is unlike Rydberg excitations. It has been shown earlier that there are empirical correlations with the position of the σ* shape-resonance and the corresponding bond length [24,60–62]. We have attempted to use this correlation for the observed blue-shift of the σ* shape-resonance in condensed nitrogen and homogeneous clusters. The blue-shift above the N 1s ionization energy is found to be considerable, since earlier work on ZEKE photoelectron spectroscopy on homogeneous nitrogen clusters has shown that the N 1s ionization energy is red-shifted by at least 0.6 eV compared to the free molecule [55]. If this red-shift in ionization energy is added to the blue-shift in σ*-energy (≈1 eV in nitrogen clusters (cf. Fig. 3)), one obtains a total blue-shift >1.5 eV. A considerable shortening of the N≡N-bond length in clusters and the condensed phase would be the implication of this result, using simple empirical bond length correlations [24]. This would imply that the N≡N-bond length decreases from 1.095 Å in the free molecule to about 1.05 Å in clusters, and even less in

the condensed phase. This change in bond length becomes smaller, if the shift in energy is referenced to the N 1s→2pπ_g(π*)-transition, since this feature is found to be almost constant in energy [53]. The resulting shortening in N≡N-bond will be at least 0.02 Å, which is also regarded to be unrealistic for Van der Waals systems, such as solid nitrogen, where a N≡N-bond length of 1.10 Å is reported from earlier experiments [63]. Therefore, energy shifts of the σ*-shape resonance cannot be treated as an indication for massive changes in bond length. Consequently, we assign the blue-shift in σ*-energy in the following on the basis of the QA approach considering dynamic properties of shape resonances.

The equivalence of atomic sites in the electronic ground state of a polyatomic molecule, which may be located in a homogeneous cluster, implies that there is an equal probability for excitations from each atom. Therefore, inner-shell excitations and subsequent photoionization processes are initiated in such systems in one of the equivalent atoms. The relevant photoelectron wave function Ψ is represented by the sum over all equivalent sites (j) [30]:

$$\Psi = \sum_j \Phi_j (t - t_j - \tau) \tag{3}$$

The different time dependences of quasi-atomic wave functions Φ_j in Eq. (3) is used to account for dynamic core–hole localization, where t_j is the beginning of core ionization. Another time dependence τ takes changes in core–hole localization into account. τ is determined by the hopping time t_h and the timescales t_e and t_n, which are characterized by the core–hole electronic decay and the relaxation of the nuclear subsystem, respectively. In addition, we introduce for shape resonances the trapping time T which corresponds to the interaction of the photoelectron with the short range molecular potential. T depends on coupling with the underlying continuum states for Rydberg excitations. Thus a competition between the various relevant timescales (t_h, t_e, t_n, and T) controls the dynamic properties of photoexcitation processes, where it is assumed that $|t_1 - t_2| \gg \max(t_h, t_e, t_n, \text{and } T)$. Two limiting cases can be distinguished, if core–hole excitations are regarded as one-electron phenomena and molecular relaxation is neglected:

$$T \ll t_h \tag{4}$$

and

$$T \gg t_h. \tag{5}$$

Approximately, $T \sim mR_{mol}v^{-1}$, where m is the multiplicity of intramolecular photoelectron scattering, v is the photoelectron velocity, and $t_h \sim (\Delta E_c)^{-1}$ [64]. ΔE_c is the energy separation between the $1\sigma_g$ and $1\sigma_u$ orbitals, where both cases allow a time independent description of the excitation. The inequality (4) is predominantly valid for core-excitation continua, where fast photoelectrons are emitted in weakly bound systems. It describes the trapped photoelectron by the molecular ion of broken symmetry, which is the result of strong core–hole localization on one of the equivalent atoms. Therefore, core-excitation of homonuclear molecules behaves similar to heteronuclear molecules, so that equivalent atomic sites can be regarded as incoherent sources of photoelectron waves. The sum of independent fluxes of electron waves from different equivalent sites is given by Eq. (6) [29,30]:

$$J \sim \sum_j |\Phi_j|^2 \tag{6}$$

Spectral changes of the flux J are due to the incoherent intramolecular interference of photoelectron waves, resulting in shape resonances in absorption and ionization cross sections.

The inequality (5) is valid for the near-edge regime (low v) in strongly bound systems (short interatomic distances). In this case, the photoelectron is trapped in the molecular ion potential, where the vacancy is delocalized as a result of fast core–hole hopping. Therefore, the symmetry of the molecular ion is quickly restored. Equivalent atomic sites are regarded in this case as equivalent, coherent sources of photoelectron waves:

$$J \sim \left| \sum_j \Phi_j \right|^2 \tag{7}$$

Hence, no contradiction between the localized and delocalized descriptions appears if core-excitations are regarded as time-dependent processes. In general, the photoelectron moves in a time-dependent potential of varying symmetry which cannot be assigned to a fixed point group. We note that these considerations are still quite crude since core–hole relaxation needs to be considered as well [65]. Auger

and radiative decays produce vacancies in upper electronic shells. These are known to be strongly delocalized in molecular systems, so that electronic relaxation tends to restore the ground state symmetry. In contrast, relaxation of nuclear subsystems tends to retain the broken molecular symmetry, since the creation of an electron–hole pair disturbs the balance of electrostatic forces keeping the ground state symmetry. The residual asymmetric force arising simultaneously with the core–hole leads to an asymmetric motion of the atoms in a molecule. This means that core–hole relaxation in molecules leads to enhancements of both localization and delocalization in shape resonances. These processes are illustrated using the example of 1s-shell photoexcitation of nitrogen in the N 1s continuum, where post-collision interaction between the photoelectron (e_{ph}) and the Auger electron (e_A) are neglected:

$$N_2 + h\nu \rightarrow N_{1s}^{+}N \rightarrow \begin{matrix} (N_2)^{++} + e_{ph} + e_A & (s) \\ (NN)^{++} + e_{ph} + e_A & (a) \end{matrix} \quad (8a)$$

The other nitrogen site is excited with the same probability:

$$N_2 + h\nu \rightarrow NN_{1s}{}^{+} \rightarrow \begin{matrix} (N_2)^{++} + e_{ph} + e_A & (s) \\ (NN)^{++} + e_{ph} + e_A & (a) \end{matrix} \quad (8b)$$

Two symmetric (s) and two asymmetric (a) channels with $D_{\infty h}$- and $C_{\infty v}$-symmetry are formed via core-excitation. These are denoted in Eq. (8a,b) as $(N_2)^{++}$ and $(NN)^{++}$, respectively. The dynamic symmetry of photoexcitation depends on the branching ratio γ between the s- and a-channels, which is obtained from ratio of fluxes in these channels (cf. Eqs. (6) and (7)). Therefore, γ corresponds to the ratio of the coherent-to-incoherent intramolecular interference of the photoelectron waves. This dynamic picture can be approximated by superimposing the excitations into symmetric and asymmetric molecular configurations, which are described in terms of quasi-stationary states [30]. Recent work on angular distributions of photoelectrons of fixed-in-space N_2 and CO_2 has shown that the N 1s- and O 1s-σ*-resonances give γ-values of ≈3.2 and ≈0.4, respectively [30]. These results are a clear indication for the fact that the photoelectron current is mainly in the symmetric channel in the case of N 1s-excited N_2, whereas this process collapses in the case of O 1s-excited CO_2. The origin of these results is found in different dynamic properties of the shape resonances [30], which are connected with the dominance of the antisymmetric stretching mode in O 1s-excited carbon dioxide [66]. The asymmetric motion is generated simultaneously with O 1s-core hole and keeps the broken inversion symmetry of the core-excited molecule, which is also reflected by specific photoemission channels. In contrast, the appearance of asymmetric $(NN)^{++}$- and $(N)^{++}$-configurations requires large interatomic separations so that they cannot be excited simultaneously with the creation of a N 1s core–hole. Evidence for this assumption comes from recent work on photoexcited oxygen [67], where it is demonstrated that low kinetic energy photoelectrons move predominantly into the asymmetric O^{+}–O-channel. This dynamic consideration is in general consistent with previous work of Miranda et al. who used a molecular orbital approach in order to take core–hole delocalization into account for the K-shell excitation of nitrogen and carbon dioxide [68].

The spectral distribution of oscillator strengths of X-ray transitions depends not as strong on γ as the angular dependence of photoelectron emission [30]. Consistently, the XANES of N_2 is properly described using for the core-excited molecular states $C_{\infty v}$- [69] and $D_{\infty h}$-symmetry [70], respectively. The γ-dependence of shape resonances in absorption is rationalized by the amplitudes $B_{lml'm'}$ as a function of γ. Considering that the delocalization of core-excitation implies the appearance of coherent sources in the surroundings, $B_{lml'm'}(\gamma)$ obeys Eq. (1) with the optical surroundings potential

$$W^{opt} = W - iU, \quad (9)$$

where negative values for the imaginary part are used [33,46]. $U(E, \gamma)$ corresponds to the increase in photoelectron flux coming from the surroundings to the absorber, where neighboring coherent sources lead to an additional phase shift β of the photoelectron waves [71]:

$$\beta = \tan^{-1}(2z + y) - \tan^{-1}(2z) - tan^{-1}(y), \quad (10)$$

where the zeroth range potential approximation to neighboring atoms $z = kW^{-1}$ and $y = UW^{-1}$ is ap-

plied. If $\beta>0$, as in the case of N_2, delocalization in the regime of shape resonances ($W>0$) leads to its red-shift, which increases with γ. Thus, one expects for the s- and a-channels that $E^{s}_{\text{shape-res}}<E^{a}_{\text{shape-res}}$. The contribution of the a-channel to the shape resonance is expected to increase in clusters ($\gamma_{\text{cluster}}<\gamma_{\text{molecule}}$). We infer from this a blue-shift for the shape resonance in nitrogen clusters relative to the transitions in the isolated molecules:

$$\epsilon \pm E_{\text{shape-res, cluster}} - E_{\text{shape-res, molecule}} > 0 \qquad (11)$$

The dominance of the symmetric channel in the N $1s^{-1}\sigma^{*}_{u}$-resonance in free nitrogen [30] allows to rationalize the large blue-shift in clusters and in the condensed phase.

The application of these considerations leads to the result, that different dynamic properties of the C 1s shape resonances in CO are obtained. Especially, the ϵ-shift does not exist for the C $1s^{-1}\sigma^{*}$-, O $1s^{-1}\sigma^{*}$-resonances in carbon monoxide and its clusters, since only the asymmetric channel is excited. These results on energy shifts in σ^{*}-resonances are in accordance with the experimental results on nitrogen and carbon monoxide clusters.

We conclude that the blue-shift of the σ^{*}-shape resonance in homogeneous nitrogen clusters and in the corresponding condensed phase is most likely not a result of a considerable change in the molecular bond length, rather than a result of dynamic properties of this continuum resonance. Consistently, bare carbon monoxide and its clusters show no spectral shift. We also note that positive values of U are responsible for a dissipation of the photoelectron waves in the surroundings [71]. The dissipation will increase in clusters and in the condensed phase and will lead to a general blue-shift of shape resonances. This is further support for the conclusion that dynamic properties dominate this spectral regime, especially since blue-shifts of the σ^{*}-shape resonance are only observed in nitrogen clusters as well as in the condensed molecule.

5. Conclusions

The experimental and theoretical study on atomic and molecular clusters in the core excitation regime has shown that several size-dependent properties are observed in partial and total yield spectra. We have shown that the $3s^{-1}np$ excitations (with $n=4, 5, 6$) in free argon clusters give rise to size dependent shifts, which do not follow a monotonous blue-shift, as in the case of the Ar 2p-Rydberg transitions. Therefore, this complicated spectral behavior cannot be assigned exclusively on the basis of experimental material. The QA approach has served to rationalize both blue- and red-shifts of the size-dependent transitions in variable size clusters. The blue-shift is due to screening of the Coulomb potential of the core-ionized atom by its neighbors, resulting in an adiabatic stressing of the atomic volume in the condensed phase, whereas a red-shift is due to the polarization of atoms in clusters and solids. 1s excitation of nitrogen and carbon monoxide clusters are also investigated in the present work. The spectral shapes are similar in the gas, clusters, and in the condensed phase. Nevertheless, the results indicate that (i) there are spectral changes in the regimes of Rydberg (Ryd) and related double excitation ($1s^{-1}Val^{-1}\pi^{*}Ryd$) and (ii) the N $1s^{-1}\sigma^{*}_{u}$-resonance is blue-shifted in clusters and in the condensed phase. This is evidently not due to molecular geometry changes. These shifts in energy are found to be a result of dynamic properties of the core-excited states. The ϵ-shift is interpreted as evidence for a dynamic phenomenon which is closely related to core–hole localization and core–hole symmetry breaking in strongly bound molecular systems with equivalent atomic sites, such as nitrogen. Specifically, it is shown that the low-symmetry cluster potential gives rise to (i) dynamic core–hole localization on one of the equivalent atoms in N_2 and (ii) incoherent intramolecular interferences of photoelectron waves at the N $1s^{-1}\sigma^{*}$-shape resonance. These changes in dynamic properties of the N $1s^{-1}\sigma^{*}_{u}$-resonance lead to a significant blue-shift in homogeneous clusters as well as in condensed nitrogen. In contrast, the localization of C 1s- and the O 1s-core hole in bare CO and its clusters does not change. Therefore there is no ϵ-shift of the shape resonance energy in free clusters compared to the molecule.

The present results can be used to predict size effects in other molecular clusters which contain small molecules with respect to dynamic properties of shape resonances. In the case of CO_2 an increase of the O $1s^{-1}$ core hole localization in clusters and in

the condensed phase is expected to occur. Hence, the O $1s^{-1}$ σ-shape resonances will be blue-shifted relative to the isolated molecule. This blue-shift is, however, expected to be smaller than in the case of free and condensed nitrogen. The C $1s^{-1}\sigma_u^*$-resonance in CO_2 is expected to be constant in energy in the free molecule, clusters, and in the condensed phase. These predictions cannot be compared to experimental results, since these have not been reported yet. We expect in general from extended experiments on 1s-shell excitations in variable size molecular clusters using high spectral resolution beam lines at state-of-the-art storage ring facilities that our predictions should be verified. We also expect that a deeper understanding with respect to the role of inelastic scattering of the primary photoelectrons by valence shell electrons will be obtained from experiments which use high spectral resolution, especially for the regime of continuum resonances.

Acknowledgements

We would like to thank C. Heinzel and S. Rabe for their help with the data acquisition of the cluster spectra. We also thank B. Wassermann, C. Hutchings, I.T. Steinberger, D. Gravel, and C.-M. Teodorescu for their help during the data acquisition of the solid samples. Financial support by the Deutsche Forschungsgemeinschaft (grant number: 436 RUS 113/339/0(R)). RFFI (grant no.: 98-03-32715), and the Fonds der Chemischen Industrie are gratefully acknowledged.

References

[1] H. Haberland (Ed.), Clusters of Atoms and Molecules I, Springer Ser. Chem. Phys. 52, Springer, Berlin, 1995.
[2] H. Haberland (Ed.), Clusters of Atoms and Molecules II, Springer Ser. Chem. Phys. 56, Springer, Berlin, 1994.
[3] S. Kakar, O. Björneholm, L. Weigelt, A.R.B. deCastro, L. Tröger, R. Frahm, T. Möller, A. Knop, E. Rühl, Phys. Rev. Lett. 78 (1997) 1675.
[4] E. Rühl, C. Heinzel, A.P. Hitchcock, H. Baumgärtel, J. Chem. Phys. 98 (1993) 2653.
[5] A.A. Pavlychev, E.V. Semenova, A.P. Hitchcock, E. Rühl, Physika B 208–209 (1995) 187.
[6] M.G. White, J.R. Grover, J. Chem. Phys. 79 (1983) 4124.
[7] H. Steger, J. de Vries, W. Kamke, I.V. Hertel, Z. Physik D 21 (1991) 85.
[8] C.Y. Ng, Adv. Chem. Phys. 52 (1983) 263.
[9] J. Stapelfeldt, J. Wörmer, T. Möller, Phys. Rev. Lett. 62 (1989) 98.
[10] J. Wörmer, M. Joppien, G. Zimmerer, T. Möller, Phys. Rev. Lett. 67 (1991) 2053.
[11] W. Kamke, J. de Vries, J. Krauss, E. Kaiser, B. Kamke, I.V. Hertel, Z. Physik D 14 (1989) 339.
[12] R. Müller, M. Joppien, T. Möller, Z. Phys. D 26 (1993) 370.
[13] J. Wörmer, R. Karnbach, M. Joppien, T. Möller, J. Chem. Phys. 104 (1996) 8269.
[14] O. Björneholm, F. Federmann, F. Fössing, T. Möller, Phys. Rev. Lett. 74 (1995) 3017.
[15] F. Federmann, O. Björneholm, A. Beutler, T. Möller, Phys. Rev. Lett. 73 (1994) 1549.
[16] E. Rühl, C. Heinzel, A.P. Hitchcock, H. Baumgärtel, H. Schmelz, C. Reynaud, W. Drube, R. Frahm, J. Chem. Phys. 98 (1993) 6820.
[17] E. Rühl, Ber. Bunsenges. Phys. Chem. 96 (1992) 1172.
[18] E. Rühl, C. Heinzel, H. Baumgärtel, M. Lavollée, P. Morin, Z. Physik D 31 (1994) 245.
[19] A. Knop, E. Rühl, in: T. Kondow, K. Kaya, A. Terasaki (Eds.), Structures and Dynamics of Clusters, Universal Academy Press, Tokyo, 1996, p. 235.
[20] A. Knop, B. Wassermann, E. Rühl, Phys. Rev. Lett. 80 (1998) 2302.
[21] A.A. Pavlychev, N.G. Fominykh, I.T. Steinberger, S. Rabe, B. Wassermann, D. Gravel, C.M. Teodorescu, E. Rühl, Surface (Russ. Acad. Nauk) 8–9 (1998) 97.
[22] A.P. Hitchcock, D.C. Mancini, J. El. Spectrosc. Relat. Phenom. 67 (1994) 1.
[23] A.P. Hitchcock, J. Electron Spectrosc. Relat. Phenom. 25 (1982) 245.
[24] J. Söhr, NEXAFS Spectroscopy, Springer, Berlin, 1992.
[25] F.A. Gianturco, M. Guidotti, U. Lamanna, J. Chem. Phys. 57 (1972) 840.
[26] J.L. Dehmer, D. Dill, A.C. Parr, in: S. McGlynn, G. Findly, R. Huebner (Eds.), Photophysics and Photochemistry in the Vacuum Ultraviolet, Reidel, Dordrecht, 1985, p. 341.
[27] J.-E. Rubensson, J. Lüning, S. Eisebitt, W. Eberhardt, Appl. Phys. A 65 (1997) 91.
[28] J. Nordgren, P. Glans, K. Gunnelin, J. Guo, P. Skytt, C. Sathe, N. Wassdahl, Appl. Phys. A 65 (1997) 97.
[29] N. Watanabe, J. Adachi, K. Soejima, E. Shigemasa, A. Yagishita, N.G. Fominykh, A.A. Pavlychev, Phys. Rev. Lett. 78 (1997) 4910.
[30] A.A. Pavlychev, N.G. Fominykh, N. Watanabe, J. Adachi, K. Soejima, E. Shigemasa, A. Yagishita, Phys. Rev. Lett. 81 (1998) 3623.
[31] A. Cesar, F.K. Gel'mukhanov, Y. Luo, H. Agren, P. Skytt, P. Glans, J.H. Guo, K. Gunnelin, J. Nordgren, J. Chem. Phys. 106 (1995) 3439.
[32] H. Agren, Y. Luo, F.K. Gel'mukhanov, Appl. Phys. A 65 (1997) 115.
[33] A.A. Pavlychev, A.S. Vinogradov, A.P. Stepanov, A.S. Shulakov, Optics and Spectrosc. 75 (1993) 327.

[34] A.A. Pavlychev, N.G. Fominykh, J. Phys. Cond. Matter 8 (1996) 2305.
[35] E. Rühl, C. Schmale, H.W. Jochims, E. Biller, M. Simon, H. Baumgärtel, J. Chem. Phys. 91 (1991) 6544.
[36] E. Holub-Krappe, C. Pettenkofer, T. Mayer, A. Schellenberger, W. Jaegermann, S. Bernstorff, F. Eggenstein, W. Peatman, in: Bessy Annual Report, 1989, p. 338.
[37] S. Bernstorff, W. Braun, M. Mast, W. Peatman, T. Schroeter, Rev. Sci. Instrum. 60 (1989) 2097.
[38] O.F. Hagena, Z. Physik D 4 (1987) 291.
[39] J. Farges, M.F. deFeraudy, B. Raoult, G. Torchet, J. Chem. Phys. 84 (1986) 3491.
[40] R. Karnbach, M. Joppien, J. Stapelfeldt, J. Wörmer, T. Möller, Rev. Sci. Instrum. 64 (1993) 2838.
[41] O.F. Hagena, W. Obert, J. Chem. Phys. 56 (1972) 1793.
[42] W.H. Adams, J. Chem. Phys. 37 (1962) 2009.
[43] T.L. Gilbert, in: Molecular Orbitals in Chemistry, Physics, and Biology, Academic Press, New York, 1972, p. 405.
[44] V. Heine, M.L. Cohen, D. Weaire, The Pseudopotential Concept, in: H. Ehrenreich, F. Seitz, T. Turnbull (Eds.), Solid State Physics. Advances in Research and Applications, Vol. 24, Academic Press, New York, 1970, p. 480.
[45] F. Calogero, The Variable Phase Approach to Potential Scattering, Academic Press, New York, 1972.
[46] V.V. Babikov, Phase Function Method in Quantum Mechanics, Nauka, Moscow, 1976.
[47] R.P. Madden, D.L. Ederer, C. Codling, Phys. Rev. 177 (1969) 136.
[48] R. Haensel, N. Kosuch, U. Nielsen, U. Rössler, B. Sonntag, Phys. Rev. B 7 (1973) 1577.
[49] A.P. Hitchcock, C.E. Brion, J. El. Spectrosc. Relat. Phenom. 18 (1980) 1.
[50] C.T. Chen, Y. Ma, F. Sette, Phys. Rev. A 40 (1989) 6737.
[51] D. Arvanitis, H. Rabus, M. Domke, A. Puschmann, G. Comelli, H. Petersen, L. Tröger, T. Lederer, G. Kaindl, K. Baberschke, Appl. Phys. A 42 (1989) 393.
[52] P. Feulner, R. Scheuerer, M. Scheuer, G. Remmers, W. Wurth, D. Menzel, Appl. Phys. A 55 (1992) 478.
[53] B. Kassühlke, P. Averkamp, P. Feulner, W. Bertholt, Phys. Rev. B 55 (1997) 10854.
[54] W.L. Jolly, K.D. Bomben, C.J. Eyermann, At. Data Nucl. Data Tab. 31 (1984) 433.
[55] E. Rühl, A.P. Hitchcock, P. Morin, M. Lavollée, J. Chim. Phys. 92 (1995) 521.
[56] R.A. Rosenberg, P.J. Love, P.R. LaRoe, V. Rehn, Phys. Rev. B 31 (1985) 2634.
[57] G.R. Wight, C.E. Brion, M.J. van der Wiel, J. El. Spectrosc. Relat. Phenom. 1 (1973) 457.
[58] E. Rühl, B. Brutschy, H. Baumgärtel, Chem. Phys. Lett. 157 (1989) 379.
[59] J. Geiger, S. Rabe, C. Heinzel, H. Baumgärtel, E. Rühl, in: L.G. Christoherou, E. Illenberger, W.F. Schmidt (Eds.), NATO-ASI Conf. Proc. Ser. B, Vol. 326, Plenum Press, New York, 1994, p. 217.
[60] F. Sette, J. Stöhr, A.P. Hitchcock, J. Chem. Phys. 81 (1984) 4906.
[61] M.N. Piancastelli, D.W. Lindle, T.A. Ferrett, D.A. Shirley, J. Chem. Phys. 86 (1987) 2765.
[62] J.A. Sheehy, T.J. Gil, C.L. Winstead, R.E. Farren, P.W. Langhoff, J. Chem. Phys. 91 (1989) 1796.
[63] T.H. Jordan, H.W. Smith, W.E. Streib, W.N. Lipscomb, J. Chem. Phys. 41 (1964) 756.
[64] G.C. King, F.H. Read, M. Tronc, Chem. Phys. Lett. 52 (1977) 50.
[65] M. Schmidtbauer, A.L.D. Kilcoyne, H.-M. Köppe, J. Feldhaus, A.M. Bradshaw, Phys. Rev. A 52 (1995) 2095.
[66] A. Kivimäki, B. Kempgens, K. Maier, H.M. Köppe, M.N. Piancastelli, M. Neeb, A.M. Bradshaw, Phys. Rev. Lett. 79 (1997) 998.
[67] A.V. Golovin, F. Heiser, C.J.K. Quayle, P. Morin, M. Simon, O. Gessner, P.-M. Guyon, U. Becker, Phys. Rev. Lett. 79 (1997) 4554.
[68] M.P. de Miranda, C.E. Bielschowsky, M.A.C. Nascimento, J. Phys. B 28 (1995) L15.
[69] A.A. Pavlychev, A.S. Vinogradov, Opt. Spectrosc. (USSR) 65 (1987) 329.
[70] J.L. Dehmer, D. Dill, J. Chem. Phys. 65 (1976) 5327.
[71] A.A. Pavlychev, J. Phys. B 32 (1999) 2077.